Nanoscale

PAPER

View Article Online
View Journal | View Issue

Cite this: *Nanoscale*, 2016, **8**, 10291

Stereo-epitaxial growth of single-crystal Ni nanowires and nanoplates from aligned seed crystals†

Hyoban Lee,[a] Youngdong Yoo,[a,b] Taejoon Kang,[c] Jiyoung Lee,[a] Eungwang Kim,[a] Xiaosheng Fang,[d] Sungyul Lee*[e] and Bongsoo Kim*[a,f]

Received 16th November 2015,
Accepted 11th April 2016

DOI: 10.1039/c5nr08080k

www.rsc.org/nanoscale

Epitaxially grown anisotropic Ni nanostructures are promising building blocks for the development of miniaturized and stereo-integrated data storage kits because they can store multiple magnetic domain walls (DWs). Here, we report stereo-epitaxially grown single-crystalline Ni nanowires (NWs) and nanoplates, and their magnetic properties. Vertical and inclined Ni NWs were grown at the center and edge regions of *c*-cut sapphire substrates, respectively. Vertical Ni nanoplates were grown on *r*-cut sapphire substrates. The morphology and growth direction of Ni nanostructures can be steered by seed crystals. Cubic Ni seeds grow into vertical Ni NWs, tetrahedral Ni seeds grow into inclined Ni NWs, and triangular Ni seeds grow into vertical Ni nanoplates. The shapes of the Ni seeds are determined by the interfacial energy between the bottom plane of the seeds and the substrates. The as-synthesized Ni NWs and nanoplates have blocking temperature values greater than 300 K at 500 Oe, verifying that these Ni nanostructures can form large magnetic DWs with high magnetic anisotropy properties. We anticipate that epitaxially grown Ni NWs and nanoplates will be used in various types of 3-dimensional magnetic devices.

1. Introduction

Ferromagnetic nanowires (NWs) have been regarded as attractive building blocks for applications in magnetic storage devices, nanoelectronics, and spintronics[1,2] because a single ferromagnetic NW with a high surface-to-volume ratio can store multiple magnetic domain walls (DWs). In particular, aligned ferromagnetic NWs can offer significant advantages for the fabrication of 3-dimensional magnetic devices such as racetrack memory.[3] Nickel (Ni), one of the representative ferromagnetic materials, has been widely used in memory chips,[4–6] magnetics,[7,8] fuel cells,[9,10] catalysts,[11–13] and batteries.[14] Because the aligned Ni NW arrays enable both miniaturization and stereo-integration of data storage kits, it is extremely important to synthesize well-aligned Ni NW arrays.

Wet-chemical approaches using anodic aluminum oxide (AAO) templates enable Ni NWs to grow vertically on a substrate.[15–17] Since these NWs are often tangled with each other and form bundles after the removal of the AAO templates, individual control of the Ni NWs in a spin device is hardly possible. In addition, Ni NWs electrochemically formed have rough surfaces, limiting efficient transport of magnetic spins and the formation of well-defined magnetic DWs. Lithographic approaches have also been employed for the fabrication of Ni NWs. However, such approaches are complex, time consuming, and expensive.[18] Recently, Chan *et al.* successfully employed chemical vapor deposition (CVD) techniques to synthesize vertical single-crystal Ni NWs on an amorphous SiO_2 substrate.[19,20] This study stimulated us to develop a morphology and growth direction controllable synthetic method of Ni nanostructures in the vapor phase.

Here, we report epitaxially grown Ni NWs and nanoplates in the vapor phase, and their magnetic properties. Vertical and inclined Ni NWs were synthesized on *c*-cut sapphire substrates and vertical Ni nanoplates were synthesized on *r*-cut sapphire substrates. The morphology and growth direction of Ni nanostructures were steered by Ni seed crystals, which were formed on the substrates by the favorable interfacial energy between the bottom plane of the seeds and the substrates.[21] In this experiment, cubic Ni seeds grew into vertical Ni NWs, tetrahedral Ni seeds grew into inclined Ni NWs, and triangular Ni seeds grew into vertical Ni nanoplates. Ni NWs and nanoplates are single-crystalline and well-faceted with atomically smooth

[a]*Department of Chemistry, KAIST, Daejeon 34141, Korea. E-mail: bongsoo@kaist.ac.kr*
[b]*Department of Chemistry, University of Minnesota, Minneapolis, Minnesota 55455, USA*
[c]*BioNanotechnology Research Center and BioNano Health Guard Research Center, KRIBB, Daejeon 34141, Korea*
[d]*Department of Materials Science, Fudan University, Shanghai 200433, P. R. China*
[e]*Department of Applied Chemistry, Kyunghee University, Kyungki-do 17104, Korea. E-mail: sylee@khu.ac.kr*
[f]*KAIST Institute for the NanoCentury, KAIST, Daejeon 34141, Korea*
†Electronic supplementary information (ESI) available. See DOI: 10.1039/c5nr08080k

surfaces. The magnetic property measurements from the vertical Ni NW and nanoplate arrays show that the blocking temperatures (T_B) are above room temperature at 500 Oe, demonstrating their suitability for potential use in future 3-dimensional magnetic memory.

2. Experimental section

2.1 Synthesis of Ni NWs and nanoplates

Ni NWs and Ni nanoplates are synthesized in a horizontal hot wall two-zone furnace employing a 1 in diameter inner quartz tube (Fig. S1†). $NiCl_2$ precursor (anhydrous, 0.02–0.04 g, 99.99%, Sigma-Aldrich) in an alumina boat is placed at the middle position of an upstream zone, and 5 × 5 mm^2 sized *c*- or *r*-Al_2O_3 substrates (MTI Corporation, USA) are placed at 15–20 cm away from the precursor. $NiCl_2$ is heated at 770–840 °C for 25 min under 80–100 sccm of Ar flow rate. In order to decompose $NiCl_2$ efficiently and prevent the oxidation of Ni nanostructures, a preheating step was accomplished at 200–300 °C.

2.2 Characterization

Field-emission SEM images were obtained on a Philips XL30S with a Pt coating to avoid a charging effect during SEM observation. TEM images including SAED patterns were obtained on a TECNAI F30 TEM operated at 200 kV. For TEM analysis, we sonicated the as-grown substrate in ethanol solution for 5 min to detach the Ni nanostructures. After Ni nanostructures were dispersed in ethanol, we dropped the solution on a holey carbon coated copper grid.

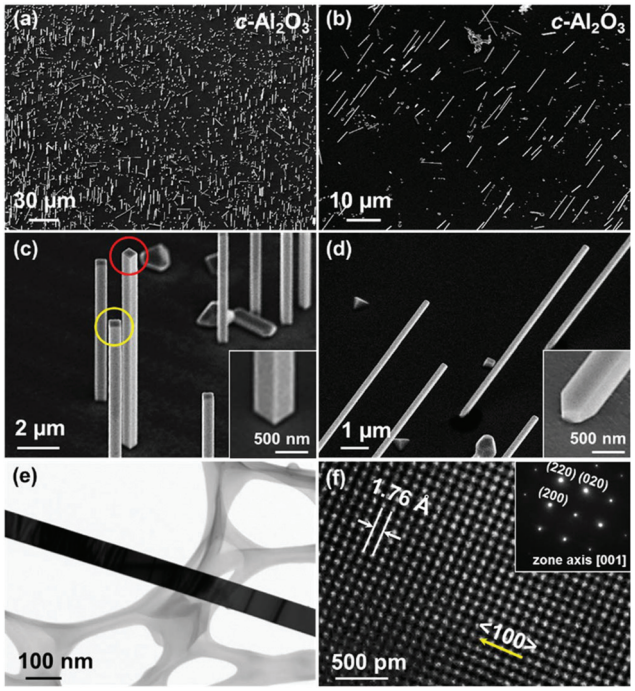

Fig. 1 45°-Tilted SEM images of (a, c) vertical and (b, d) inclined Ni NWs on *c*-Al_2O_3 substrates. The Ni NWs have well-defined facets, 100–500 nm diameters, ~10 μm lengths, and rectangular parallelepiped shapes. Magnified SEM image of the vertical Ni NWs shows that they have two types of orientations with an angle of 45° (yellow and red circles). The insets show the bottom end structures of the Ni NWs. The different bottom end structures of the vertical and inclined Ni NWs suggest that they are grown from different seed crystals. (e, f) HRTEM image and SAED patterns of Ni NWs clearly indicate that the Ni NWs are single-crystalline and have a growth direction of <100>.

3. Results and discussion

3.1 Ni NW synthesis of epitaxially grown Ni nanostructures in the vapor phase

Ni NWs and nanoplates were epitaxially synthesized on *c*-cut sapphire (*c*-Al_2O_3) and *r*-cut sapphire (*r*-Al_2O_3) substrates, respectively, using a horizontal quartz tube furnace system (Fig. S1†). Anhydrous $NiCl_2$ was employed as a precursor and a simply modified van Arkel method was used for the separation and purification of Ni.[22,23] In the quartz tube, $NiCl_2$ is evaporated, transported to the sapphire substrates by a carrier gas, and decomposed into Ni and Cl_2. After a reaction time of 25 min, single-crystalline Ni NWs and nanoplates are grown on *c*-Al_2O_3 and *r*-Al_2O_3 substrates, respectively.

3.2 Vertical and inclined Ni nanowires on *c*-Al_2O_3 substrates

Fig. 1a–d show scanning electron microscopy (SEM) images of vertical and inclined Ni NWs on *c*-Al_2O_3 substrates. The vertical Ni NWs were grown at the center of the substrate, and the inclined NWs were grown at the edges (Fig. S2†). Both NWs are rectangular parallelepipeds having a diameter of 100–500 nm and a length of ~10 μm. The diameter can be controlled by changing the source temperature or reaction time. The vertical Ni NWs exhibited two orientations with an angle of 45°, as marked by the yellow and red circles in Fig. 1c. The insets in Fig. 1c and d show the different bottom end structures of the vertical and inclined Ni NWs, indicating that the vertical and inclined Ni NWs grew from different seed structures. Distinct lattice fringes and selected-area electron diffraction (SAED) patterns obtained *via* transmission electron microscopy (TEM) confirm that the Ni NWs are single-crystalline and have a growth direction of <100> (Fig. 1e and f).

To investigate the Ni NW growth mechanism, we observed Ni seeds around the Ni NWs on *c*-Al_2O_3 substrates. Cubic Ni seed crystals are observed around the vertical Ni NWs (Fig. 2a). Similar to the vertical Ni NWs, cubic Ni seeds have two orientations with an angle of 45° (inset of Fig. 2a). The same alignments and tip structures of the vertical Ni NWs and cubic Ni seed crystals suggest that the vertical Ni NWs grow from the cubic Ni seed crystals. Fig. 2b is a cross-sectional TEM image of a single cubic Ni seed on a *c*-Al_2O_3 substrate. The sample was fabricated using focused ion beam (FIB) milling, and the yellow dashed line in Fig. 2a is the cut direction. From the cross-sectional TEM analysis, we observed that the cubic Ni seed crystal is enclosed by {100} facets and is single-crystalline without any internal twin planes.

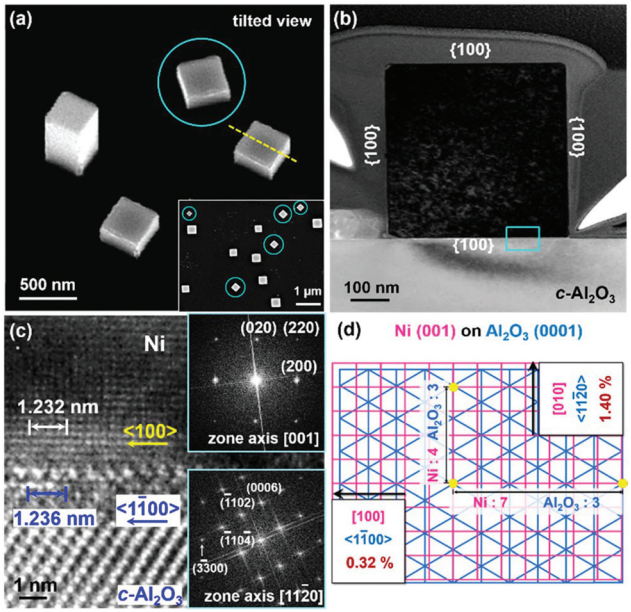

Fig. 2 (a) 35°-Tilted SEM image of cubic Ni seed crystals on a *c*-Al_2O_3 substrate. The cubic Ni seed crystals have two types of orientations with an angle of 45°. The inset is a top-view SEM image of cubic Ni seed crystals. (b) Cross-sectional TEM image of a cubic Ni seed crystal after it was cut along the yellow dashed line in (a). (c) HRTEM image and FFT patterns of the cyan square region in (b). The lattice spacing of the Ni (100) planes is 1.76 Å and that of the Al_2O_3 (1$\bar{1}$00) planes is 4.12 Å. (d) Schematic of the atomic planes at the epitaxial interface between the Ni (001) and Al_2O_3 (0001) planes.

Fig. 2c shows a high-resolution TEM (HRTEM) image and fast Fourier transform (FFT) patterns of the cyan square region in Fig. 2b. The Ni (100) plane is formed epitaxially on the Al_2O_3 (0001) plane. The schematic of the atomic planes at the epitaxial interface between Ni (001) and Al_2O_3 (0001) planes shows that the interfacial energy between these two planes is highly favorable (Fig. 2d). Seven layers of Ni and 3 layers of Al_2O_3 have a 0.32% domain-matched misfit along the Ni [100]//Al_2O_3 <1$\bar{1}$00> direction (the lattice spacing of the Ni (100) planes is 1.76 Å and that of the Al_2O_3 (1$\bar{1}$00) planes is 4.12 Å).[24,25] Additionally, 4 layers of Ni and 3 layers of Al_2O_3 have a 1.40% domain-matched misfit along the Ni [010]//Al_2O_3 <11$\bar{2}$0> direction (the lattice spacing of the Ni (010) planes is 1.76 Å and that of the Al_2O_3 (11$\bar{2}$0) planes is 2.38 Å). These small lattice mismatches enable the epitaxial formation of cubic Ni seed crystals on the substrate, leading to the vertical growth of Ni NWs. Meanwhile, when the Ni (001) plane is rotated to an angle of 45°, domain-matched misfits of 0.32% and 4.03% appear along the Ni [110]//Al_2O_3 <1$\bar{1}$00> and Ni [$\bar{1}$10]//Al_2O_3 <11$\bar{2}$0> directions, respectively (Fig. S3†). This fair domain matching epitaxy can cause the formation of 45°-rotated Ni seed crystals, as shown in the cyan circles of Fig. 2a. The result of the domain matching epitaxy explains well the two orientations of the cubic Ni seed crystals and further confirms that the vertical Ni NWs grow from cubic Ni seeds.

Around the inclined Ni NWs, tetrahedral Ni seed crystals are observed. Fig. 3a and b show top view and 35°-tilted SEM images of tetrahedral Ni seeds. As shown in the red and yellow circles of Fig. 3a, the tetrahedral Ni seed crystals have two types of orientations and both Ni seeds are mirror images of each other. Fig. 3c is a 35°-tilted SEM image of short inclined Ni NWs. The same alignments and tip structures of the inclined Ni NWs and tetrahedral Ni seed crystals suggest that the inclined Ni NWs grow from tetrahedral Ni seeds. Fig. 3d is a cross-sectional TEM image of a single tetrahedral Ni seed crystal cut along the yellow dashed line in Fig. 3a. This result shows that the tetrahedral Ni seed crystal is enclosed by {100} side facets and a (111) bottom plane. Fig. 3e shows a HRTEM image and the FFT pattern of the cyan square region in Fig. 3d, which suggests that the Ni (111) plane is formed epitaxially on the Al_2O_3 (0001) plane. The schematic of the atomic planes at the epitaxial interface between the Ni (111) and Al_2O_3 (0001) planes shows that the misfits of 4.42% and 4.41% appear along the Ni <1$\bar{1}$0>//Al_2O_3 <11$\bar{2}$0> and Ni <11$\bar{2}$>//Al_2O_3 <1$\bar{1}$00> directions, respectively (Fig. 3f, the lattice spacing of the Ni (1$\bar{1}$0), Al_2O_3 (11$\bar{2}$0), Ni (11$\bar{2}$), and Al_2O_3 (1$\bar{1}$00) planes are 2.49 Å, 2.38 Å, 4.31 Å, and 4.12 Å, respectively). The lattice mismatches of 4.42% and 4.41% are substantial. Nevertheless,

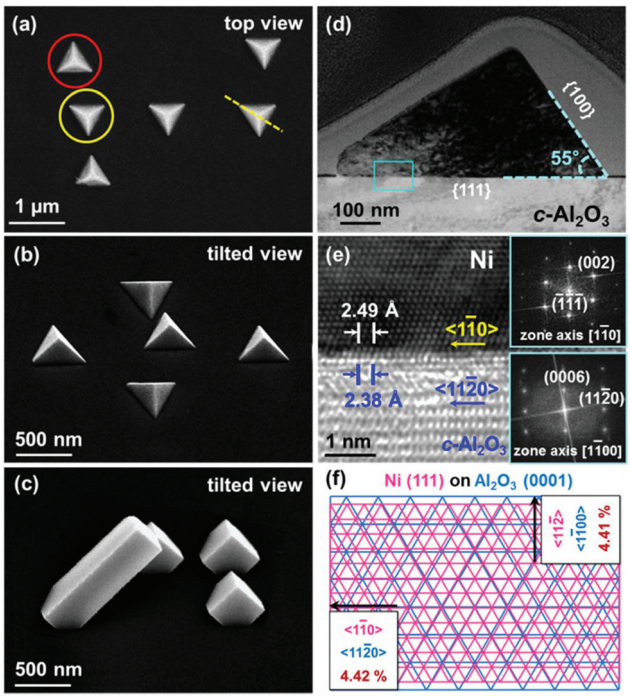

Fig. 3 (a) Top-view and (b) 35°-tilted SEM images of tetrahedral Ni seed crystals on a *c*-Al_2O_3 substrate. Tetrahedral Ni seed crystals have two types of orientations as marked by the red and yellow circles in (a). (c) 35°-Tilted SEM image of the short inclined Ni NWs. (d) Cross-sectional TEM image of a tetrahedral Ni seed crystal after it was cut along the yellow dashed line in (a). (e) HRTEM image and FFT patterns of the cyan square region in (b). The lattice spacing of the Ni (1$\bar{1}$0) planes is 2.49 Å and that of the Al_2O_3 (11$\bar{2}$0) planes is 2.38 Å. (f) Schematic of atomic planes at the epitaxial interface between the Ni (111) and Al_2O_3 (0001) planes.

tetrahedral Ni seed crystals are formed on the c-Al_2O_3 substrates because the same 3-fold symmetry of the Ni (111) and Al_2O_3 (0001) planes significantly reduce the interfacial energy between them.[26,27]

We tried to find intermediate steps between tetrahedral Ni seeds and inclined Ni NWs. Ni nanocrystals in Fig. S4(b, d, f) and (a, d, e)† have very similar geometries and alignments as well as the same crystallographic structures, suggesting that the inclined Ni NWs grow from these Ni nanocrystals. The tilt angle of the inclined Ni nanorods to the substrate is measured as 55°, which is the supposed tilt angle of the NWs.

The deposition flux, substrate temperature, and local flow conditions are the key experimental conditions, strongly depending on the location of the substrate. Ni vapor flux is nearly perpendicular to the substrate at the center of the substrate, whereas turbulent vapor flow might occur at the edge of the substrate.[22] When the Ni vapor flux direction is perpendicular to the substrate, vertical growth from the cubic seed could be more favored than inclined growth from the tetrahedral seed because of more favorable solid angle of collision for the NW growth. Inclined NW growth could be more favored near the edge because of the turbulent flow.

3.3 Vertical Ni nanoplates on r-Al_2O_3 substrates

Ni nanoplates were vertically synthesized on r-Al_2O_3 substrates (Fig. 4a). The well-faceted Ni nanoplates are isosceles triangle shaped with 5–8 μm of bottom lengths and 2–4 μm of heights. Some of the Ni nanoplates are rotated by 86°, as shown in Fig. 4b. Fig. 4c–e show TEM and HRTEM images and the FFT pattern of a single Ni nanoplate. Distinct lattice fringes and a single set of face-centered cubic (fcc) Ni structures clearly confirm the single-crystallinity of the Ni nanoplates. The growth direction of vertical Ni nanoplates is [110]. The X-ray diffraction (XRD) patterns of both the Ni NWs and Ni nanoplates exhibit the same peaks, corresponding well with the fcc Ni structure (JCPDS 7440-02-0, Fig. S5†).

On the Ni nanoplate grown r-Al_2O_3 substrates, triangular Ni seed crystals are observed. Fig. 5a and its inset are 35°-tilted and top view SEM images of the triangular Ni seed crystals. The cyan dashed lines in Fig. 5a show that the triangular Ni seeds have two orientations with an angle of 86°. These orientations correspond to the vertical Ni nanoplates in Fig. 4b. The same alignments of vertical Ni nanoplates and triangular Ni seed crystals suggest that the vertical Ni nanoplates grow from the triangular Ni seeds. Fig. 5b is a cross-sectional TEM image of a single triangular Ni seed crystal cut along the yellow dashed line in Fig. 5a. The triangular Ni seed crystal is single-crystalline and enclosed by {100} side facets and a (110) bottom plane. The HRTEM image and FFT patterns of the cyan square region in Fig. 5b show that the Ni (110) plane is formed epitaxially on the Al_2O_3 ($\bar{1}012$) plane. Two layers of Ni and 1 layer of Al_2O_3 have a 0.57% domain-matched misfit along the Ni <001>//Al_2O_3 <02$\bar{2}$1> direction (Fig. 5d, the lattice spacing of the Ni (001) plane is 1.76 Å and that of the Al_2O_3 (02$\bar{2}$1) plane is 3.50 Å). Additionally, 7 layers of Ni and 5 layers of Al_2O_3 have a 0.40% domain-matched misfit along the Ni <110>//Al_2O_3 <2$\bar{2}$01> direction (Fig. 5d, the lattice spacing of

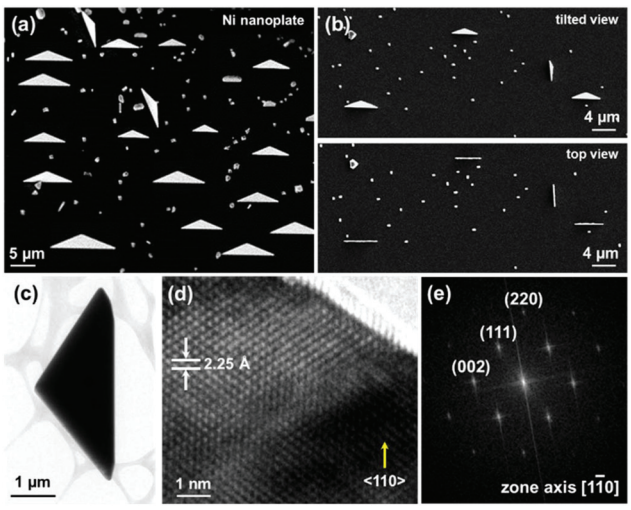

Fig. 4 (a) 35°-Tilted SEM images of vertical Ni nanoplates on an r-Al_2O_3 substrate. Well-faceted Ni nanoplates have 5–8 μm bottom lengths, 2–4 μm heights, and isosceles triangle shape. (b) 35°-Tilted (upper) and top-view (lower) SEM images of vertical Ni nanoplates show that they have two types of orientations with an angle of 86°. (c) TEM and (d) HRTEM images and (e) FFT patterns of a Ni nanoplate show distinct lattice fringes and a single set of fcc Ni structure, verifying the single-crystallinity of the Ni nanoplates.

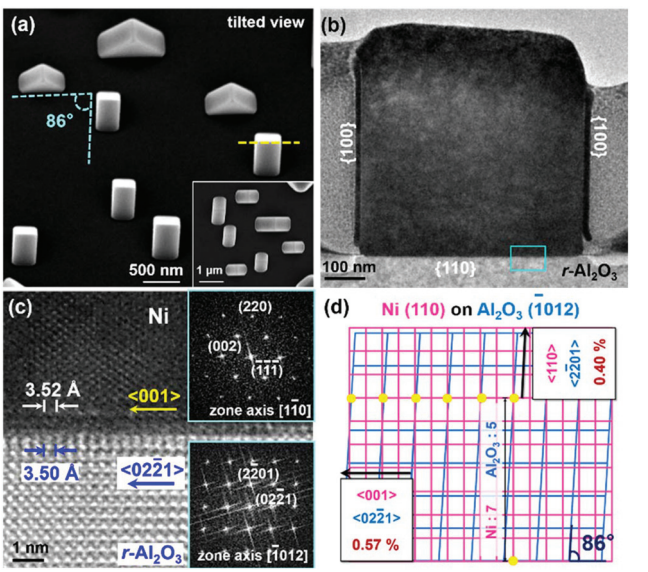

Fig. 5 (a) 35°-Tilted SEM image of triangular Ni seed crystals on an r-Al_2O_3 substrate. Triangular Ni seed crystals have two types of orientations with an angle of 86°. The inset is a top-view SEM image of the triangular Ni seed crystals. (b) Cross-sectional TEM image of a triangular Ni seed crystal after it was cut along the yellow dashed line in (a). (c) HRTEM image and FFT patterns of the cyan square region in (b). The lattice spacing of the Ni (001) planes is 1.76 Å and that of the Al_2O_3 (02$\bar{2}$1) planes is 3.50 Å. (d) Schematic of the atomic planes at the epitaxial interface between the Ni (110) and Al_2O_3 ($\bar{1}$012) planes.

the Ni (110) planes is 2.49 Å and that of the Al_2O_3 $(2\bar{2}01)$ planes is 3.50 Å). These domain-matched misfits are small enough to form the triangular Ni seed crystals on *r*-Al_2O_3 substrates. Furthermore, the Al_2O_3 $(02\bar{2}1)$ and Al_2O_3 $(2\bar{2}01)$ planes have the same lattice spacing and they are angled 86° to each other. Therefore, Ni atoms can settle equally along the Ni <001>//Al_2O_3 <$02\bar{2}1$> and Ni <001>//Al_2O_3 <$2\bar{2}01$> directions, which is why the vertical Ni nanoplates have two orientations with an angle of 86° on *r*-Al_2O_3 substrates (Fig. S7†).

We propose the following explanation for the growth mechanism of vertical Ni NWs, inclined Ni NWs, and vertical Ni nanoplates. The anisotropic growth of Ni nanostructures could be induced by the anisotropic environment that provides anisotropic flows of Ni vapor to the seed crystals, as we reported previously on noble metal NWs.[24] In the current experiment, the $NiCl_2$ precursor can decompose to Ni vapor and chloride gas at 700 °C and 1 atm. Ni atoms colliding with the substrate nucleate to form small seed crystals, of which bottom planes are well matched with the lattice plane of the substrates. Ni atoms then directly deposit onto the pre-formed seed crystals or indirectly approach the seed crystals through surface diffusion after they first collide on the sapphire substrates. Since most of Ni NWs and Ni nanoplates are formed in vertical or inclined orientations on Al_2O_3 substrates, we suggest that direct impingement from the vapor is dominant when the substrate temperature is 850–900 °C. As we increased the substrate temperature higher than 1000 °C, vertically grown Ni nanobelts were formed on *c*-Al_2O_3 substrates (Fig. S8†), and these nanobelts were thought to be formed by the lateral growth of Ni NWs due to increased surface diffusion of Ni atoms. When we increased the initial amount of $NiCl_2$ precursor by three times (other experimental conditions were unchanged), Ni NWs were grown horizontally on *c*-Al_2O_3 substrates while short Ni nanorods were grown on *r*-Al_2O_3 substrates (Fig. S9†). These observations suggest that we can adjust the orientation of Ni nanostructures by controlling the magnitude of the deposition flux, which determines the dominant material flux direction toward the seed and thus the growth direction.

3.4 Magnetic property of vertical Ni nanowires and nanoplates

The magnetic properties of the vertical Ni NWs and the Ni nanoplates were investigated using superconducting quantum interference device (SQUID) measurements. Fig. 6a and b are the *M*–*H* curves of vertical Ni NWs and nanoplates at 300 K. The curves show distinct magnetic hysteresis due to the structural anisotropy of the vertical Ni NWs and nanoplates. $Ni^{\parallel}$ means that the external magnetic field is oriented in the parallel direction to the vertical Ni nanostructures, and $Ni^{\perp}$ means that the external magnetic field is oriented in the perpendicular direction to the vertical Ni nanostructures. In both the applied field directions, the vertical Ni NWs and nanoplates exhibit typical ferromagnetic behavior. According to the previous literature, natural thin nickel-oxide layers may induce additional magnetic anisotropy *via* the exchange-bias effect at the ferromagnetic/antiferromagnetic interface (Fig. S10†).[28,29]

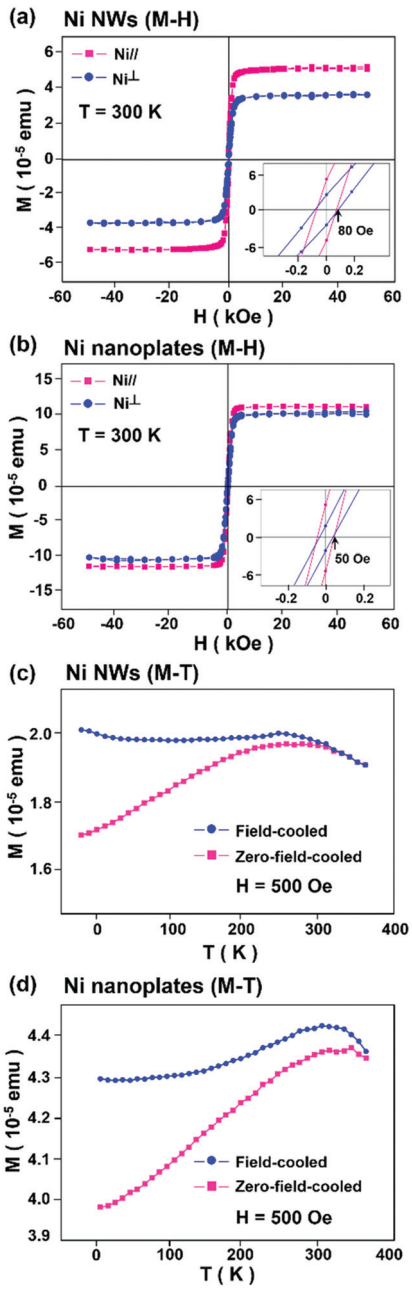

Fig. 6 *M*–*H* curves of vertical (a) Ni NWs and (b) nanoplates collected at 300 K. Distinct magnetic hysteresis loops are clearly shown. $Ni^{\parallel}$ and $Ni^{\perp}$ imply that the external magnetic field is oriented in the parallel or perpendicular direction relative to the vertical Ni nanostructures. The insets of (a, b) are magnified hysteresis loops. The coercivity values of the Ni NWs and the nanoplates are 80 and 50 Oe. The *M*–*T* curves of the vertical (c) Ni NWs and (d) nanoplates show that they have T_B values greater than 300 K at 500 Oe.

The insets of Fig. 6a and b are magnified hysteresis loops of the vertical Ni NWs and the nanoplates, showing that the coercivity values of the NWs and nanoplates are 80 and 50 Oe, respectively. Importantly, the *M*–*T* curves of vertical Ni NWs and nanoplates show that the as-synthesized Ni nanostructures have blocking temperatures (T_B) greater than 300 K

under an external magnetic field of 500 Oe (Fig. 6c and d). In previous reports, Ni nanoparticles with diameters of a few nanometers and triangular Ni nanoplates with edge lengths of ~15 nm exhibited T_B values of ~31 K and ~226 K at 500 Oe, respectively.[30–32] Our single-crystalline Ni NWs and nanoplates are much larger than these nanostructures and have a very clean surface without surfactants, thus they can form relatively large magnetic DWs and have strong magnetic anisotropy properties. Xu *et al.* reported that Ni nanoplatelets show T_B values higher than nanoparticles, which may be ascribed to the large size as well as good crystallinity.[33]

Our vertical Ni NWs and nanoplates exhibit enhanced coercive force as a reflection of the magnetic shape anisotropy at room temperature compared with that of the bulk one (*ca*. 0.7 Oe). Single crystalline Ni NWs synthesized here also show higher magnetic properties than polycrystalline Ni NWs that can be considered as random-anisotropy ferromagnets, of which local uniaxial anisotropy competes with the interatomic exchange and external fields.[34]

4. Conclusions

We developed the morphology and growth direction controllable synthetic method of Ni nanostructures in the vapor phase. By using this method, vertical Ni NWs, inclined Ni NWs, and vertical Ni nanoplates were successfully synthesized on sapphire substrates. The morphology and growth direction of Ni nanostructures are determined by Ni seed crystals. Cubic Ni seeds grew into vertical Ni NWs, tetrahedral Ni seeds grew into inclined Ni NWs, and triangular Ni seeds grew into vertical Ni nanoplates. Furthermore, vertical Ni NWs and nanoplates have blocking temperature values greater than 300 K at 500 Oe, verifying that these Ni nanostructures can form large magnetic DWs with high magnetic anisotropy properties. We expect that stereo-aligned Ni NWs and nanoplates will contribute to the development of 3-dimensional magnetic devices.

Acknowledgements

This research was supported by the Public Welfare & Safety Research Program (NRF-2012M3A2A1051682, NRF-2012M3A2A1051686) and NRF grant (2013R1A2A2A01069073), the Global Frontier Project through the Center for BioNano Health-Guard (H-GUARD_2014M3A6B2060489) funded by MSIP, and KRIBB initiative Research Program. H. L. is the recipient of End Run Project funded by KAIST (N01150074). TEM analysis was performed at KBSI in Daejeon.

References

1 G. A. Prinz, *Science*, 1998, **282**, 1660–1663.
2 A. Brataas, A. D. Kent and H. Ohno, *Nat. Mater.*, 2012, **11**, 372–381.
3 S. S. P. Parkin, M. Hayashi and L. Thomas, *Science*, 2008, **320**, 190–194.
4 I. Takeuchi, O. O. Famodu, J. C. Read, M. A. Aronova, K.-S. Chang, C. Craciunescu, S. E. Lofland, M. Wuttig, F. C. Wellstood, L. Knauss and A. Orozco, *Nat. Mater.*, 2003, **2**, 180–184.
5 J. Cui, Y. S. Chu, O. O. Famodu, Y. Furuya, J. Hattrick-Simpers, R. D. James, A. Ludwig, S. Thienhaus, M. Wuttig, Z. Zhang and I. Takeuchi, *Nat. Mater.*, 2006, **5**, 286–290.
6 Y. Tanaka, Y. Himuro, R. Kainuma, Y. Sutou, T. Omori and K. Ishida, *Science*, 2010, **327**, 1488–1490.
7 I. S. Lee, N. Lee, J. Park, B. H. Kim, Y. W. Yi, T. Kim, T. K. Kim, I. H. Lee, S. R. Paik and T. Hyeon, *J. Am. Chem. Soc.*, 2006, **128**, 10658–10659.
8 V. Bonanni, S. Bonetti, T. Pakizeh, Z. Pirzadeh, J. Chen, J. Nogués, P. Vavassori, R. Hillenbrand, J. Åkerman and A. Dmitriev, *Nano Lett.*, 2011, **11**, 5333–5338.
9 A. Atkinson, S. Barnett, R. J. Gorte, J. T. S. Irvine, A. J. McEvoy, M. Mogensen, S. C. Singhal and J. Vohs, *Nat. Mater.*, 2004, **3**, 17–27.
10 J. R. Wilson, W. Kobsiriphat, R. Mendoza, H.-Y. Chen, J. M. Hiller, D. J. Miller, K. Thornton, P. W. Voorhees, S. B. Adler and S. A. Barnett, *Nat. Mater.*, 2006, **5**, 541–544.
11 G. W. Huber, J. W. Shabaker and J. A. Dumesic, *Science*, 2003, **300**, 2075–2077.
12 A. L. Goff, V. Artero, B. Jousselme, P. D. Tran, N. Guillet, R. Métayé, A. Fihri, S. Palacin and M. Fontecave, *Science*, 2009, **326**, 1384–1387.
13 S. Scheller, M. Goenrich, R. Boecher, R. K. Thauer and B. Jaun, *Nature*, 2010, **465**, 606–608.
14 C. D. Wessells, S. V. Peddada, R. A. Huggins and Y. Cui, *Nano Lett.*, 2011, **11**, 5421–5425.
15 X. W. Wang, G. T. Fei, X. J. Xu, Z. Jin and L. D. Zhang, *J. Phys. Chem. B*, 2005, **109**, 24326–24330.
16 H. Pan, B. Liu, J. Yi, C. Poh, S. Lim, J. Ding, Y. Feng, C. H. A. Huan and J. Lin, *J. Phys. Chem. B*, 2005, **109**, 3094–3098.
17 C. M. Hangarter and N. V. Myung, *Chem. Mater.*, 2005, **17**, 1320–1324.
18 F. Li, M. Zhu, C. Liu, W. L. Zhou and J. B. Wiley, *J. Am. Chem. Soc.*, 2006, **128**, 13342–13343.
19 K. T. Chan, J. J. Kan, C. Doran, L. Ouyang, D. J. Smith and E. E. Fullerton, *Nano Lett.*, 2010, **10**, 5070–5075.
20 K. T. Chan, J. J. Kan, C. Doran and L. Ouyang, *Philos. Mag.*, 2012, **92**, 2173–2186.
21 N. Liakakos, C. Achkar, B. Cormary, J. Harmel, B. Warot-Fonrose, E. Snoeck, B. Chaudret, M. Respaud, K. Soulantica and T. Blon, *ACS Nano*, 2015, **9**, 9665–9677.
22 Y. Yoo, S. Han, M. Kim, T. Kang, J. In and B. Kim, *Chem. – Asian J.*, 2011, **6**, 2500–2505.
23 A. E. van Arkel and J. H. Boer, *Z. Anorg. Allg. Chem.*, 1925, **148**, 345–350.
24 Y. Yoo, K. Seo, S. Han, K. S. K. Varadwaj, H. Kim, J. Ryu, H. Lee, J. Ahn, H. Ihee and B. Kim, *Nano Lett.*, 2010, **10**, 432–438.

25 J. Narayan and B. C. Larson, *J. Appl. Phys.*, 2003, **93**, 278–285.
26 T. Nakamura, H. Minoura and H. Muto, *Thin Solid Films*, 2002, **405**, 109–116.
27 G. Dehm, M. Rühle, G. Ding and R. Raj, *Philos. Mag. B*, 1995, **71**, 1111–1124.
28 N. Bagkar, K. Seo, H. Yoon, J. In, Y. Jo and B. Kim, *Chem. Mater.*, 2010, **22**, 1831–1835.
29 V. Salgueiriño-Maceira, M. A. Correa-Duarte, M. Bañobre-López, M. Grzelczak, M. Farle, L. M. Liz-Marzán and J. Rivas, *Adv. Funct. Mater.*, 2008, **18**, 616–621.
30 M. J. Bonder, E. M. Kirkpatrick, T. Martin, S.-J. Kim, R. D. Rieke and D. L. Leslie-Pelecky, *J. Magn. Magn. Mater.*, 2000, **222**, 70–78.
31 Y. Leng, Y. Li, X. Li and S. Takahashi, *J. Phys. Chem. C*, 2007, **111**, 6630–6633.
32 C. L. Yuan, *J. Phys. Chem. C*, 2010, **114**, 2124–2126.
33 R. Xu, T. Xie, Y. Zhao and Y. Li, *Cryst. Growth Des.*, 2007, **7**, 1904–1911.
34 M. Zheng, L. Menon, H. Zeng, Y. Liu, S. Bandyopadhyay, R. D. Kirby and D. J. Sellmyer, *Phys. Rev. B: Condens. Matter*, 2000, **62**, 12282–12286.